Title

Walker-A Motif Acts to Coordinate ATP Hydrolysis with Motor Output in Viral DNA Packaging

Journal

Journal of Molecular Biology, 428(13)

ISSN

0022-2836

Authors

delToro, Damian
Ortiz, David
Ordyan, Mariam
et al.

Publication Date

2016-07-01

DOI

10.1016/j.jmb.2016.04.029

Peer reviewed

HHS Public Access

Author manuscript

J Mol Biol. Author manuscript; available in PMC 2017 July 03.

Published in final edited form as:

J Mol Biol. 2016 July 3; 428(13): 2709–2729. doi:10.1016/j.jmb.2016.04.029.

Walker-A motif acts to coordinate ATP hydrolysis with motor output in viral DNA packaging

Damian delToro[1,*], **David Ortiz**[2,*], **Mariam Ordyan**[1], **Jean Sippy**[3], **Choon-Seok Oh**[3], **Nicholas Keller**[1], **Michael Feiss**[3,†], **Carlos E. Catalano**[2,4,†], and **Douglas Smith**[1,†]

[1]Department of Physics, University of California, San Diego, La Jolla CA 92093

[2]Department of Medicinal Chemistry, University of Washington, Seattle, WA 98195

[3]Department of Microbiology, Roy J. and Lucille A. Carver College of Medicine, University of Iowa, Iowa City, IA 52242, USA

Abstract

During assembly of many viruses a powerful ATP-driven motor translocates DNA into a preformed procapsid. A Walker-A "P-loop" motif is proposed to coordinate ATP binding and hydrolysis with DNA translocation. We use genetic, biochemical, and biophysical techniques to survey the roles of P-loop residues in bacteriophage lambda motor function. We identify 55 point mutations that reduce virus yield to below detectible levels in a highly sensitive genetic complementation assay and 33 that cause varying reductions in yield. Most changes in the predicted conserved residues K76, R79, G81, and S83 produce no detectible yield. Biochemical analyses show that R79A and S83A mutant proteins fold, assemble, and display genome maturation activity similar to wild-type, but exhibit little ATPase or DNA packaging activity. Kinetic DNA cleavage and ATPase measurements implicate R79 in motor ring assembly on DNA, supporting recent structural models that locate the P-loop at the interface between motor subunits. Single-molecule measurements detect no translocation for K76A&R, while G81A and S83A exhibit strong impairments consistent with their predicted roles in ATP binding. We identify eight residue changes spanning A78-K84 that yield impaired translocation phenotypes and show that Walker-A residues play important roles in determining motor velocity, pausing, and processivity. The efficiency of initiation of packaging correlates strongly with motor velocity. Frequent pausing and slipping caused by changes A78V and R79K suggest these residues are important for ATP alignment and coupling of ATP binding to DNA gripping. Our findings support recent structural models implicating the P-loop arginine in ATP hydrolysis and mechanochemical coupling.

Graphical abstract

[†]Correspondence to: des@ucsd.edu, carlos.catalano@ucdenver.edu, michael-feiss@uiowa.edu.

[4]Current Address, Department of Pharmaceutical Sciences, Skaggs School of Pharmacy and Pharmaceutical Sciences, University of Colorado Denver, Aurora, CO 80045

[*]These authors contributed equally

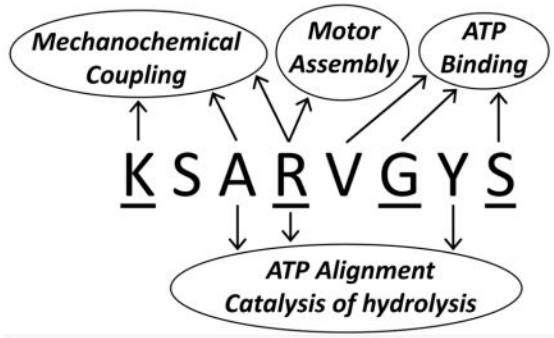

Keywords

Viral DNA Packaging Motor; Terminase; Optical Tweezers; ATPase; Mutagenesis of Walker A Motif

INTRODUCTION

Many double-stranded DNA viruses utilize a molecular motor during assembly to package their genomes into preformed procapsid shells. The genome is recognized, cut from a polymeric precursor, and translocated into the shell to a density approximating that of crystalline DNA (1). Measurements of single DNA molecule packaging with optical tweezers show that these motors generate very high forces (>50 pN) and translocate DNA rapidly with high processivity (typically <1 slip per kbp packaged) (2–12). Average translocation rates range from ~150 bp/s for phage phi29 up to ~700 bp/s for phage T4 (measured at low procapsid filling, low force, saturating ATP, and room temperature). The phi29 motor was shown to translocate in coordinated bursts of four 2.5 bp steps coincident with phosphate release (13). These motors also exhibit occasional pauses, which are typically a few seconds in duration and occur roughly once per kbp of DNA packaged.

While much is understood about the function of these motors, their structural and biochemical mechanisms are not completely understood, and a number of different models have been proposed (14–20). The DNA translocase activity resides in the viral terminase enzyme. Terminases generally are heterooligomers of a small subunit (TerS) involved in genome recognition and a large subunit (TerL) with an N-terminal ATPase domain and C-terminal endonuclease domain (20–23). In the present work we study phage lambda. Its terminase proteins assemble into protomers containing two TerS (gpNu1) and one TerL (gpA) subunits (Figure 1) (24). In solution the protomer is in slow equilibrium with a tetramer of protomers that assemble into a ring-like complex, albeit at elevated concentration (K_D= 4 μM) (25, 26). However, at physiological concentrations and in the presence of either ATP or IHF, four protomers will assemble at the lambda DNA *cos* site (K_D= 20 nM) to afford a maturation complex that “matures” the genome end (i.e. cleaves and separates the DNA–complex I) in preparation for packaging (Yang, et al., submitted). Binding of complex I to the portal vertex of a procapsid is followed by DNA translocation (Fig. 1). The tetrameric stoichiometry is retained in the post-cleavage complex (complex I) and is likely maintained in the translocating packaging motor complex (Yang, et al., in preparation).

Atomic structures of the large terminase subunits of phages T4 and Sf6 and of the ATPase domains of those of phages P74-26 and phi29 (14, 17, 18, 27) show that their ATPase center‘s fold belongs to a large group of oligomeric translocases, the ASCE (Additional Strand Catalytic Glutamate) superfamily (28, 29). This superfamily includes many cellular ATPases having diverse functions including protein unfolding and degradation; protein transport and translocation; ATP synthesis; and DNA recombination, unzipping, transport, and translocation (28, 29). Studies of viral terminases may therefore provide information that is broadly relevant to understanding many ATP-powered machines (30, 31).

The core of the ATPase center is a five-stranded parallel β-sheet with α-helical segments connecting the β-strands. Two ATP-interacting amino acid segments, the Walker A (P-loop) and B motifs, have characteristic sequences. The classical Walker A signature sequence is (G/A)XXXXGK(T/S), where “X” can be any amino acid (32). Extensive studies show that the serine/threonine hydroxyl coordinates the Mg^{2+} of Mg^{2+}-ATP, and the lysine‘s ε-amino group coordinates the β– and γ– phosphates of ATP, positioning them for hydrolytic attack (31, 33–38). Recent structural studies of phi29 also found that the C-terminal glycine is also involved in coordinating the phosphates of a bound nucleotide (AMP-PNP) (27). The downstream Walker B segment, whose signature sequence is ΦΦΦΦD, has four hydrophobic residues (indicated by “Φ”) followed by an aspartate carboxyl group that also coordinates the Mg^{2+} of the Mg^{2+}-ATP complex. Together, the Walker A and B segments position the β– and γ– phosphates for nucleophilic attack by an activated water molecule provided by a “catalytic” glutamate carboxylate group. In the ACSE ATPases, including terminases, this glutamate immediately follows the aspartate (28, 39, 40).

Upstream of Walker A are residues forming the adenosine binding pocket (41). For phage λ’s terminase, crosslinking studies identified an ATP-binding center in the N-terminus of the large subunit, gpA, by showing that residues Y46 and K84 were crosslinked by 8-azido-ATP (Figure 1) (42). Nonconservative changes in residue Y46 yielded no detectable DNA packaging or ATPase activity in bulk *in vitro* experiments. Subsequent work further showed that a mutant terminase with the conservative Y46F change had only mild impairments of DNA packaging and packaging ATPase activities, indicating a strong coupling of the high-affinity ATPase activity to DNA translocation (43, 44). Further evidence for an N-terminal ATP-binding domain in lambda gpA was provided by a genetic screen for missense mutations producing endonuclease-competent and DNA packaging defective mutants. This screen identified a set of 10 mutations affecting this domain (45), one of which (K76R) is a predicted Walker-A residue.

Genetic and bioinformatic work by Rao and co-workers identified key components of the ATPase center of T4’s terminase subunit, gp17, including the adenine binding, Walker A, and Walker B segments (40, 46). Sequence alignments enabled prediction of the locations of these centers in the terminases of other DNA bacteriophages and identified an atypical Walker A sequence for λ and some other viral terminases, being 76-KSARVGYS-83 in the case of lambda (Table 1). Notably, this segment lacks the C-terminal lysine in the classical Walker A “GK(T/S)” sequence normally implicated in phosphate binding but has a lysine at the N-terminus of the P-loop that appears to be conserved among a subset of viral terminases (termed “Deviant I” or “N-lys” Walker A motifs). Structural modeling led to the proposal

that this lysine, instead of the one in the classical position, coordinates the β– and γ–phosphates and that S83 (in the classical motif position) coordinates the Mg^{2+} ion (47).

Sequence alignments show that most terminase Walker A motifs also contain an arginine not present in the classical motif, corresponding to R79 in lambda gpA (46). All tested residue changes of this arginine in phage T4 terminase were found to be lethal (48). Various critical roles have been proposed for this arginine based on recent structural studies. Studies of T4 terminase suggest it is an “arginine finger” that triggers ATP hydrolysis by interacting with the β- and γ-phosphates to stabilize the transition state (14). Data on Sf6 terminase supports this but also suggests it has a distinct role in mechanochemical coupling (17). The arginine’s side chain is proposed to interact with a “linker” domain between N- and C-terminal domains to couple hydrolysis to DNA translocation. Studies of phage P74-26 terminase suggest that the Walker A arginine is involved in both mechanochemical coupling and hydrolysis but not specifically acting as an arginine finger (18). In this case, the P-loop arginine and an adjacent residue are proposed to interact with a C-terminal “lid” domain and cause the N-terminal domain to rotate and translocate DNA. Thus, there is significant controversy as to the roles of specific Walker A motif residues in ATP hydrolysis and its coupling to DNA translocation, a central function of all terminases.

Here, we use a combination of genetic, biochemical, and biophysical approaches to investigate the role of Walker A residues in the lambda motor function. Initially we sought to identify mutants exhibiting altered DNA translocation phenotypes to serve as tools for studying the motor mechanism. To this end, we first used a genetic assay to survey effects on phage yield of 88 single residue changes spanning the motif. A subset of these mutants that exhibited varying levels of impairment was chosen for more detailed biophysical and biochemical investigation. These studies identified four mutant enzymes that exhibited no DNA translocation and eight with varying partially-impaired translocation phenotypes. Our findings show that Walker A residues play important roles in determining motor velocity, processivity, and pausing. The data support the prediction that conserved residues K76, G81 and S83 play critical roles in phosphate/Mg^{2+} binding. Our findings also provide support for recent models which predict that the conserved Walker-A arginine (R79) is involved in mediating coupling of the ATP hydrolysis cycle to DNA gripping and translocation (17, 18).

RESULTS AND DISCUSSION

Genetic Analysis

To investigate the roles of gpA’s identified Walker A residues, we mutagenized individual codons of the 76-KSARVGYSK-84 segment to create a collection of missense mutants. In total we produced 88 different mutants with residue changes spanning the Walker A motif. Although K84 is not considered part of the motif, it was included in this study because the crosslinking results indicate that it is ATP-interacting. To ascertain the level of terminase function we developed a highly sensitive genetic complementation assay to quantify the effect of point mutations altering gpA on viral assembly. Briefly, a plasmid supplies altered or wild type (WT) gpA protein to a prophage whose production of WT gpA is blocked by amber mutations. If the supplied gpA is sufficiently functional fully-assembled phages are produced, with yields reflecting the degree of impairment, and these phages are detected via

a sensitive plaque-counting assay. To enable plaque growth during this detection stage, production of WT gpA from the phage genome is turned on by use of an amber suppressor bacterial strain. With this assay we can detect phage yields for mutants as low as 10^{-7} –fold lower than that produced when WT gpA is supplied in the complementation assay (Fig. 2).

This complementation assay is advantageous over directly introducing gpA mutations into the viral genome, because for a λ strain to produce a plaque its yield must be greater than ~10% that of WT in our experience. Accordingly mutations that produce a lower yield in our complementation assay may be regarded as “lethal” from a genetic point of view (those labeled non-green in Fig. 2). Notably, all but 3 Walker A mutants out of the 88 tested were lethal. Importantly, however, our assay can provide evidence for viral assembly, and hence translocation activity, even for lethal changes. This approach is more sensitive than previous methods used to screen phage T4 terminase Walker-A mutants, which only distinguished lethal vs. non-lethal changes (49).

Our assays revealed significant impairments in response to all changes across every identified Walker A residue (Fig. 2). Moreover, changes in conserved residues K76, R79, G81, and S83, caused the strongest impairments, with most resulting in no detectible phage yield. Even chemically conservative changes G81A and S83T caused significant impairments. These findings are consistent with the predicted crucial roles of these residues in ATP binding, hydrolysis, and/or mechanochemical coupling, as reviewed in the introduction. In contrast, non-conserved residues S77, A78, V80, and Y82 were more tolerant to changes in that they caused less impairment and tolerated more substitutions, both conservative and nonconservative. K84, just outside the identified motif, was the most tolerant to substitutions. Altogether, these results strongly support the Walker A motif assignments.

Altogether we identified 55 mutants exhibiting no detectible phage yield (those labeled grey in Fig. 2) and 33 mutants with reduced yield (non-grey labels). We considered the latter mutants good candidates for further characterization as they may have impairments in DNA translocation that could shed light on motor function. To our knowledge this is the most extensive collection of such mutants identified for any Walker A motif.

Biophysical Analysis

We complement the wide genetic survey described above with targeted biophysical and biochemical studies on selected mutants. The genetic assays allow us to survey effects of many different residue changes on impairment on viral assembly. However, there can potentially be many different causes of these impairments. For example, a mutation could affect not only translocation but also folding of the TerL protein, multimeric assembly with TerS, DNA binding and cleavage, interaction with the procapsids, etc (Fig. 1). Even if translocation is primarily affected, it can be affected in many different possible ways and for many possible reasons. For example, there may be no translocation at all, or partly impaired translocation, such as slow translocation, or more frequent slips and/or pauses. Such defects may potentially be caused by factors such as impaired ATP binding, hydrolysis, and product release, and/or problems with mechanochemical coupling. Importantly, a mutant may be very strongly or even completely impaired in viral assembly yet still exhibit DNA

translocation activity with phenotypic impairments that can shed light on the roles of residues in motor function.

To measure the effect of residue changes on DNA translocation we used optical tweezers measurements of single DNA molecule packaging (3). In this technique proheads are attached to a microsphere trapped with optical tweezers. A single DNA molecule attached to a second trapped microsphere is packaged into one of the proheads, causing the two microspheres to be pulled together (Fig. 3A). A feedback system controls the separation between the two traps so as to apply a force of 5 pN to keep the DNA stretched, allowing the length of DNA packaged vs. time to be tracked. Further details are given in the methods section and prior publications (3, 8, 44, 50–53). We sought to identify altered translocation phenotypes that would give insights on the roles of P-loop residues in the motor mechanism. Since the single-molecule measurements are time consuming, we selected 12 mutants from among the 88 investigated in the genetic studies. The chosen residue changes span all eight P-loop residues and an adjacent residue (K84). We first chose mutants for which the genetic assays revealed an intermediate impairment in phage yield (those labeled orange in Fig. 2, i.e. S77V, A78V, V80A, Y82A, and K84A). For residues where the genetic assays showed greater impairments (labeled pink), those with some detectable phage yield were studied (G81A and S83T). For the predicted conserved residues where almost all changes were severely lethal (no detectable phage yield, labeled grey) we studied mutants with a change to the relatively inert alanine (K76A, R79A, and S83A). We also examined chemically-conservative changes K76R and R79K.

To give the mutant motors the best chance to show activity most of the measurements were made under the “least taxing” conditions, with saturating ATP, low load force, and low capsid filling (3, 44, 50). In the end, we identified eight mutants with partially-impaired translocation and four with no detectable translocation. The partly-impaired mutants exhibited a wide range of phenotypes with differences in efficiency of initiation of packaging, packaging rates, pausing, and slipping, thus implicating these residues as playing important and variable functional roles in translocation (Figs. 3–5). Initiation efficiencies (relative rates at which single packaging events were detected; see methods) ranged from 5% to 90% of that for WT and average packaging rates ranged from 4% to 86% of that for WT (Fig. 4).

Comparison with the Genetic Studies—Consistent with the genetic studies, DNA translocation impairments were generally greater in response to changes in the predicted conserved residues, suggesting that the impairments in phage yield are attributable, at least in part, to translocation defects. Changes to residues K76, R79, G81, and S83, except for the conservative change S83T, showed either no packaging events or very few with very slow packaging rates (Fig. 4). These findings are consistent with biochemical studies, discussed below, showing strongly impaired packaging and ATPase activities for mutants R79A and S83A, and our previous finding that K76R does not package DNA (54). Smaller impairments were observed in response to changes in residues A78, V80, and Y82, identified as non-conserved, and residue K84 just outside the motif. That changing K76 causes much stronger impairment than changing K84, the only other lysine in the region,

clearly shows that K76 is the critical lysine despite having an atypical position in the motif, in accord with predictions (46).

However, there were a few notable differences between the genetic and single-molecule findings. No translocation was detected for S77V but a small phage yield was observed (Fig. 4), indicating that packaging and viral assembly can proceed to completion, albeit inefficiently. Our interpretation is that change S77V reduces initiation efficiency to below that which can be detected by the single-molecule assay and that S77 can be implicated as playing an important role in initiation efficiency. We note that it is possible to detect phage yield but not translocation in the single molecule assay because the phage yield assay has higher sensitivity. It can detect virus assembly activity at levels down to 10^7-fold lower than WT. In the single-molecule assay we probe for complexes one-at-a-time and it is only feasible to conduct ~1000 trials, so if the initiation efficiency is less than ~1 per 1000 we may not detect any events.[i] Although S77 was not previously highlighted as a conserved residue, a serine appears at this position in several other phage terminases (e.g., Table 1), so it may be conserved in a subset of terminases.

Conversely, mutants R79K and S83A showed some DNA translocation activity but no detectable phage yield and conservative change S83T caused only a small reduction in translocation activity but a large reduction in phage yield. Our interpretation is that residues R79 and S83 are less critical for initiation and packaging at low filling densities, but may have a defect in the completion of packaging. Specifically, packaging may initiate but fail to complete if the residue change affects the motor's force-generating capability. To test this idea, we measured mutant S83T with a 5× higher load force (25 pN) and found that its packaging rate indeed decreases more sharply with increasing load compared with WT. Specifically, at 25 pN, WT packages with an average motor velocity of 41 ± 5 bp/s while S83T yields 27 ± 4 bp/s.

Implications of Motor Slipping—Studies show that the phi29 motor translocates in 2.5 bp steps per ATP hydrolyzed (13). This parameter has not been measured for lambda, but our prior studies set an upper bound of 8 bp based on energetic considerations (3). Translocation is occasionally interrupted by pauses and slips for both WT and mutant motors but these events do not occur every translocation step; e.g., even for the mutant that slipped most frequently, A78V, ~100 bp were packaged on average per slip (Fig. 4). Therefore, these events must be off pathway states from the main mechanochemical cycle. To characterize the on pathway, hydrolysis-coupled translocation rate we define "motor velocity" to be the packaging rate not including pauses and slips. Mean motor velocities range from 42 to 340 bp/s for the mutants versus 400 bp/s for WT. The observed packaging rate for WT (350 bp/s) is only slightly lower than the motor velocity, indicating only modest effects of pauses and slips. In contrast, for some of the mutants packaging rate is significantly lower than motor velocity due to increased pausing and slipping (Fig. 4).

[i]It is also possible that initiation is more efficient *in vivo* than *in vitro*. It is possible that the 5 pN force could stall translocation of a mutant, but this would not explain why S77V produces a small phage yield, because to produce a phage the whole genome has to be packaged and the estimated force needed to package more than 90% of the genome length is ~20–30 pN (3, 56).

Since one of the expected roles of the P-loop is to mediate ATP phosphate binding we considered whether the slowed motor velocities caused by residue changes could be attributed to slowed progression to hydrolysis. Before hydrolysis, ATP must first diffuse to the binding site, which we will refer to as “loosely docked ATP” as in recent publications on the phi29 motor (13, 55). The rate of loose docking depends on [ATP] and accessibility of the binding site. The ATPase must then react by undergoing a conformational change that positions the ATP for hydrolysis, which has been referred to as “tight binding” (56) (13). Studies of phi29, and measurements we present below for lambda, indicate that this transition causes the motor to grip DNA tightly (56). In principle both transitions may be affected by mutations in the Walker A residues. Thus, the residence time in the apo or loosely-docked ATP states, where DNA grip is weak, can be varied by changing [ATP] and may be affected by residue changes.

To investigate the effect of increasing this residence time, we measured WT with [ATP] lowered from 0.5 mM (saturating) to 5 and 2.5 μM; note that the K_m for ATP hydrolysis is ~5 μM (57, 58)). We observe decreased motor velocity and increased slipping, consistent with increased residence time in an apo state with weak DNA grip. If a residue change were to slow progression to hydrolysis we would expect it to follow the same trend of increasing slipping with decreasing motor velocity. As shown in Figs. 4 & 5A we find that mutants V80A, G81A, and S83A are consistent with this trend. These findings support the prediction that residues G81 and S83 play crucial roles in ATP docking and/or binding. On the other hand, mutants S83T, K84A, A78V, Y82A, R79K, do *not* follow this trend (Fig. 5A). For example, mutant A78V has higher velocity than WT with 5 μM ATP, yet slips much *more* frequently, while mutant Y82A has much lower velocity that WT with saturating ATP, yet slips much *less* frequently. Increased residence time in the apo or loosely-docked ATP states would not account for the impairments exhibited by these mutants. The slowed motor velocities of these mutants suggests impairments in different processes, either ATP hydrolysis, ADP/P_i release, and/or the conformational change which drives translocation.

Residues Involved in Mechanochemical Coupling—Of the five mutants whose defects could not be accounted for by slowed progression to hydrolysis, R79K and A78V are particularly notable in that with saturating ATP they exhibit significantly more frequent slipping than WT. This finding provides support for recent structural models that implicate the P-loop arginine and an adjacent residue in mechanochemical coupling (17, 18) because a defect in coupling would be expected to cause slipping. Conformational changes in the P-loop are proposed to mediate interactions with other subdomains of TerL that result in a “lever”-like motion to translocate the DNA. Tight ATP binding causes the lever to “cock” and grip DNA. After hydrolysis and P_i and ADP release, TerL is proposed to return to its initial conformation, resulting in DNA translocation. In Sf6 terminase the P-loop arginine appears to interact with a residue in a linker region between the globular N- and C-terminal subdomains, and this linker and the C-terminal domain are proposed to interact with DNA (17). In P74-26 terminase P-loop arginine R39 and the adjacent residue Q40 appear to interact with residues in a C-terminal “lid” subdomain above the ATPase active site (18). A rotation of the lid with respect to an N-terminal DNA binding region is proposed to drive translocation. Our finding that a change to arginine (R79) causes increased slipping supports

both of these models. That a mutation to an adjacent residue (A78V) also increases slipping suggests that R79 and A78 could play an analogous role to R39 and Q40 in P74-26. The slow motor velocity exhibited by mutant R79K is also consistent with models that implicate this arginine as playing a critical role in the ATP hydrolysis step of the cycle.

Mutants with Increased Processivity—While A78V, R79K, and V80A exhibited more frequent slipping than WT, mutants Y82A and S83T actually exhibit significantly *less* frequent slipping than WT (Fig. 4 &5A). This increase in motor processivity could be regarded as a "gain in function" caused by the residue change. However, the motor velocities are reduced and WT, Y82A, and S83T all have such high processivities that slipping does not significantly affect their packaging rates. A possible explanation for the reduced slipping is that changes Y82A and S83T may *decrease* the residence time in the apo and/or loosely-docked ATP states where DNA grip is weak, while the reduction in motor velocity is caused by impairments in ATP hydrolysis, ADP/P_i release, and/or the conformational change which drives translocation.

Causes of Motor Pausing—Akin to the trend observed with slipping, WT measurements with varying [ATP] show that pausing frequency increases with decreasing motor velocity (Fig. 5B). These pauses could be due to transitions from the apo state, in which the motor often resides at low [ATP], to an off-pathway pause state in which the motor grips the DNA tightly despite not binding ATP tightly. Mutants V80A, G81A, S83A exhibit pausing consistent with this trend (Fig. 5B), suggesting increased residence time in the apo or loosely-docked ATP states, which agrees with the conclusion we reached based on their slipping. Mutants A78V, Y82A, and S83T are not consistent with this trend (Fig. 5B), again in agreement with the conclusion we reached based on their slipping. This implies that slowed progression to hydrolysis cannot account for the pausing exhibited by these mutants; it also would not account for the pausing exhibited by mutant R79K (since, as we explained above, it would not account for its slipping).

As with their slipping, mutants Y82A and S83T exhibit less frequent pausing than WT, again consistent with *decreased* residence time in the apo and/or loosely-docked ATP states (from which pauses and slips are prone to occur). In contrast, mutants A78V and R79K exhibit significantly more frequent pauses than WT, implying that their pauses must be attributed to a different off-pathway pause state. It is also notable that their mean pause duration is ~2-fold longer than that measured for WT. A plausible structural mechanism for such pausing would be tight binding of ATP in a misaligned orientation such that it cannot be rapidly hydrolyzed and must realign or dissociate before packaging can proceed. This would implicate residues A78 and R79 as playing important roles in proper ATP alignment.

Efficiency of Initiation of Packaging Correlates with Motor Velocity—Overall, our measurements with WT and mutant terminases reveal a strong correlation (Pearson correlation coefficient R=0.73, P=0.03) between motor velocity and efficiency of initiation of packaging (a measure of the rate at which packaging events were detected; see methods). The implication is that high motor velocity is important for efficient initiation, potentially to minimize DNA release that could occur when only a small length of DNA is packaged. This model bears some analogy to promoter clearance events where RNA polymerase must

synthesize primers of sufficient length to allow the enzyme to clear the promoter for efficient mRNA synthesis (59). Studies of phi29 and SPP1 show that the portal channel has a highly electronegative inner surface (60, 61). During initiation, this charge may present an energy barrier that inhibits the negatively charged DNA from entering the channel. A similar effect was observed in recent studies of phage T4 in which fluorescence imaging was used to measure packaging of multiple short (45 bp) DNAs (62). The average time between re-initiation events increased with decreasing [ATP] and with a residue change that reduced the ATP hydrolysis rate. It was proposed that this effect may serve to regulate packaging to limit initiation under suboptimal nutritional conditions. Our findings provide broader support for these hypotheses. However, the correlation between initiation efficiency and motor velocity is not strict. Mutant Y82A is a notable exception, as it exhibits low motor velocity but high initiation efficiency. Our finding that Y82A also exhibits ~5-fold lower slipping than WT suggests that high processivity can compensate for the low motor velocity in initiation.

Biochemical Analysis

To complement the genetic and biophysical studies described above, we chose two severely impaired mutants, R79A and S83A, for further study by biochemical methods; the K76R mutant was characterized previously (54). The genetic assays found that all tested changes of these three residues resulted in no measureable phage yield, with the exception of chemically conservative change S83T. The single-molecule assays showed no translocation activity with K76R or R79A and only two packaging events were recorded with S83A in hundreds of trials, making it difficult to define the mechanistic nature of their defects. Prior biochemical characterization of K76R terminase demonstrated that this mutation abrogates DNA packaging activity *in vitro*, consistent with the unmeasurable phage yield *in vivo* and with the absence of packaging activity in the single-molecule studies. Interestingly, however, we found that the ATPase activity of the enzyme is little affected (63). This indicates that mechanochemical coupling between ATP hydrolysis and DNA translocation is severely impaired, and implicates residue K76 in the coupling. Here we utilize similar biochemical approaches to examine the effect of residue changes at critical Walker A residues R79 and S83.

Folding and Self-Assembly of the Mutant Terminase Enzymes—To define the role of individual residues in a biochemical experiment, residue changes would ideally be “surgical” in that they would affect ATPase and/or translocation activities with little effect on protein folding, native self-assembly, and/or DNA maturation activities. The mutant R79A and S83A proteins express and purify similarly to WT and exhibit similar yields with no evidence of aberrant aggregation (data not shown); this indicates that the mutations do not grossly affect the structures of the enzymes. To confirm this, we employed circular dichroism (CD) spectroscopy and found that neither mutation affects the far-UV CD spectrum or thermal stability (Fig. S1A,S1B), indicating that the secondary and tertiary structures of the mutant proteins remain intact.

We next examined the quaternary structures of the mutant enzymes using a sedimentation velocity analytical ultracentrifugation (SV-AUC) approach; the results demonstrate that both mutant enzymes retain a stable heterotrimeric $TerL_1$•$TerS_2$ stoichiometry throughout

purification and during prolonged storage (not shown), confirming that the mutations do not affect quaternary interactions required for protomer assembly. The functional enzyme requires further assembly into a catalytically-competent ring tetramer (24, 26, 63, 64) and we next confirmed that neither residue change affects the protomer-tetramer equilibrium using SV-AUC. Consistent with published results, the WT-terminase protomer establishes an equilibrium between the protomer (5S) and the assembled ring tetramer (~15S) and the SV-AUC data demonstrate that both mutant enzymes similarly establish this slow, but dynamic equilibrium (Fig. 6).

DNA Maturation Activities—Terminases possess a site specific nuclease activity that is necessary for "maturing" the genome end in preparation for DNA packaging (Fig. 1). For the mutations to have a surgical effect on ATPase/translocation activities, assembly of the maturation complex and "*cos*-cleavage" nuclease activity must remain intact and similar to that of the WT enzyme. We presumed that this would be the case because endonuclease activity resides in a distinct C-terminal domain, separated from the N-terminal Walker A motif by a linker domain. Notwithstanding, we confirmed this hypothesis using a *cos*-cleavage endonuclease assay. The product of this reaction (P_4•D_L•D_R, where P_4 represents the ring of 4 terminase protomers and D_L•D_R represent the cleaved duplex products) is very stable ($T_{1/2}$= 8 hours) which results in a single-turnover reaction (63). The reaction time course is thus described by a simple single-turnover, monophasic exponential model,

$$F = A * [1 - \exp(-k_{obs} * \tau)] \quad (1)$$

where F is the fraction of DNA cleaved at time (τ), A is the extent of the reaction at infinite time, and k_{obs} is the observed rate constant for the reaction.

Analysis of the *cos*-cleavage reaction according to Equation 1 shows that the S83A mutant only has modest decrease in k_{obs} relative to WT (Fig. 7, Table 2). In contrast, *cos*-cleavage by the R79A mutant is significantly slowed. Moreover, the reaction time course shows a prominent lag in product formation (Fig. 7) and is poorly described by the simple single-turnover model. We therefore considered a 3-state model that includes a slow, reversible protomer assembly step prior to catalysis,

$$4 * \mathrm{P} + cos\mathrm{DNA} \underset{k_{-1}}{\overset{k_1}{\rightleftharpoons}} \mathrm{P}_4 \bullet cos\mathrm{DNA} \xrightarrow{k_2} \mathrm{P}_4 \bullet \mathrm{D}_\mathrm{L} \bullet \mathrm{D}_\mathrm{R} \quad (2)$$

where P represents the protomer in solution, P_4•*cos*DNA represents pre-nicking complex composed of four protomers assembled on the *cos*DNA substrate (Fig. 1), k_1 is the rate constant for tetramer assembly, k_{-1} is the rate constant for tetramer disassembly, k_2 is the rate constant for the irreversible chemical step (duplex nicking), and D_L•D_R represent the cleaved duplex products. As shown in Fig. 7, the *cos*-cleavage time course for the R79A mutant is well described by this 3-state model with improved goodness-of-fit parameters as described in *Methods*, and affords the rate constants presented in Table 2. Notably, k_1 is

significantly slower than that expected of a diffusion controlled DNA binding reaction (~ 10^7–10^8 M^{-1}•sec^{-1}) (65), consistent with an attenuated assembly step; this hypothesis is directly tested below.

In the above studies, the *cos*-cleavage reactions were initiated by adding terminase to the reaction mixture and duplex nicking thus requires several kinetic steps including (i) assembly of a catalytically-competent complex at the *cos*-site and (ii) subsequent nicking of the duplex, as depicted in Fig. 1 and described kinetically in Equation 2. For WT terminase, the pre-nicking complex (P_4•*cos*DNA) is very stable ($T_{1/2}$= 12 hours; k_{-1}= 1.6 × 10^{-5} sec^{-1}) (66) and the assembly reaction is essentially irreversible on the timescale of the experiment. Thus, when duplex nicking (k_2) is fast, the model simplifies to the monophasic model (Eq. 1), as observed for the wild-type enzyme. We considered that the lag observed with the R79A mutant might result from altered assembly kinetics (k_1/k_{-1}) and we directly tested this hypothesis using a modified experimental approach. The R79A mutant enzyme was pre-incubated with *cos*-DNA for 15 minutes to allow terminase to assemble at the *cos* site (P_4•*cos*DNA) and the reaction was then initiated with the addition of Mg^{2+}. Under these conditions, the lag disappears and the resulting kinetic time course is well described by a monophasic exponential model (Equation 1) (Fig. 7). Analysis of the data yields a k_{obs} essentially identical to that of the S83A mutant and only ~1.5 fold less than that of WT (Table 2). These data indicate that the R79A mutation only modestly affects the rate of duplex nicking by the enzyme, but rather affects assembly of a catalytically-competent nuclease complex (P_4•*cos*DNA), either due to an impairment in DNA binding and/or a subsequent conformational rearrangement required for duplex nicking. This is discussed further below.

DNA Packaging Activities—The genetic and biophysical data presented above suggest that the severe impairments in phage yield caused by residue changes R79A and S83A are related to functional defects in DNA packaging. To directly test this hypothesis, packaging of a full lambda genome length substrate was investigated using a DNase protection assay (67, 68). As anticipated, the packaging activities of the mutant enzymes are severely impaired (Fig. 8A); R79A and S83A terminases package only (3.6 ± 1.4) % and (1.6 ± 0.8) % of the input DNA relative to WT, respectively. Thus, the data confirm that these residues are indeed crucial for DNA packaging. Notably, although no packaging events were detected with R79A in the single-molecule assay, it exhibited strongly reduced but detectable packaging activity in the ensemble assay. This finding demonstrates the advantage of using these two complementary techniques—while the single molecule assay can provides more detail on translocation dynamics, the ensemble assay can provide higher sensitivity to detect very low levels of packaging.

Packaging ATPase Activities—Translocation by the terminase ring complex must be linked to ATP hydrolysis by TerL. Since the residues we changed are critical Walker A residues at the packaging ATPase site, it would be anticipated that these changes severely impair ATP hydrolysis, and thus packaging; however, prior characterization of the K76R mutant enzyme demonstrates that while packaging activity is abrogated by this mutation, ATPase activity is little affected (54). We therefore examined steady-state ATP hydrolysis by

R79A and S83A mutants. Indeed, we found that the steady-state ATPase activity of both is strongly impaired, with only (1.5 ± 0.1) % and (0.7 ± 0.1) % activity relative to WT, respectively (Fig. 8A and Table 3). These impairments directly account for the severe defects in the DNA packaging activities caused by the residue changes, as predicted.

The ATPase Defects of R79A and S83A Have Different Mechanisms—To further probe the mechanism responsible for impairments in ATP hydrolysis caused by these residue changes, we performed single turnover kinetic measurements. Unlike the steady state conditions employed above, single-turnover studies employ an enzyme concentration in *excess* of the substrate (ATP). This isolates catalytic steps leading up to and including the chemical step of the enzyme-catalyzed reaction (i.e., kinetics of ATP binding, conformational changes, and chemical hydrolysis), but not post-chemistry events, such as ADP release. We first examined single turnover ATP hydrolysis where the reaction was initiated with the addition of terminase to the reaction mixture. As anticipated, we find that ATP hydrolysis by the WT enzyme is well described by a monophasic exponential time course[ii] (Fig. 8B) where k_{obs}= (0.123 ± 0.001) sec^{-1} (Table 4). Consistent with the steady-state results, change S83A causes a severe ~680-fold reduction in the rate of the reaction (Fig. 8B, Table 4).

The R79A mutation also causes a significant impairment, albeit less than that caused by S83A, and its reaction time course additionally shows a clear lag in product formation (Fig. 8B). These data fit poorly to a single exponential time course (not shown) and we therefore considered a model that incorporates a slow reversible step prior to hydrolysis.

$$4*\mathrm{P}+\mathrm{DNA}+\mathrm{ATP}\underset{k_{-1}}{\overset{k_1}{\rightleftharpoons}}\mathrm{P}_4\bullet\mathrm{DNA}\bullet\mathrm{ATP}\overset{k_2}{\rightleftharpoons}\mathrm{P}_4\bullet\mathrm{DNA}\bullet\mathrm{ADP}\bullet\mathrm{P_i} \quad (3)$$

where P represents the protomer in solution, P_4•DNA•ATP represents the catalytically competent tetramer assembled on DNA, k_1 is the rate constant for tetramer assembly, k_{-1} is the rate constant for tetramer disassembly, and k_2 is the rate constant for the chemical step (ATP hydrolysis). Note that this model simplifies to the monophasic one when k_1 is fast. As a check, we first analyzed the kinetic data for WT terminase, holding k_2 (ATP hydrolysis rate) to the experimentally determined value of k_{obs}= 0.123 sec^{-1} (Table 4) and allowed k_1 to float during the fit. This yields k_1= (1.0 ± 0.65) ×10^6 $M^{-1}s^{-1}$, consistent with a partially diffusion controlled fast step prior to chemical hydrolysis (Table 4) (65) and provides confidence that the model adequately describes the data.

We next analyzed the data for R79A allowing both parameters to float; this yields k_1= (1.32 ± 0.9) ×10^4 $M^{-1}s^{-1}$ and k_2= (5.3 ± 2.9) × 10^{-3} sec^{-1} with improved goodness-of-fit parameters over the simple monophasic model as described in *Methods*. As anticipated, k_2 has been significantly slowed (23-fold), consistent with an effect on the chemical ATP hydrolysis step. This is consistent with the findings of the single-molecule studies described

[ii]Equation 1 where F= fraction of ATP hydrolyzed at time τ.

above and with recent structure-based models (14, 17, 18) that suggest R79 plays an important role in facilitating ATP hydrolysis in *cis*. Additionally, k_1 has been significantly slowed (75-fold), which is responsible for the observed kinetic lag. Previous work in our group suggests that activation of packaging ATPase activity is directly related to assembly of the ring tetramer complex[iii] (24–26, 63). Since we demonstrated above that R79A possesses a subtle DNA assembly defect in the *cos*-cleavage reaction (Fig. 7), we considered the possibility that a similar assembly defect might be responsible for the observed lag in single turnover ATPase activity. To directly test this hypothesis, R79A was pre-incubated with DNA for 15 minutes to allow complex assembly and the reaction was then initiated with ATP. The data presented in Figure 8B demonstrate that, under these conditions, the kinetic lag disappears and the data are well described by a simple monophasic time course (Equation 1), which affords $k_{obs} = (4.9 \pm 0.6) \times 10^{-3}$ sec^{-1}, a 25-fold decrease in the rate of ATP hydrolysis relative to WT enzyme (Table 4). Importantly, k_{obs} obtained in this experiment is in agreement with k_2 (the chemical step) obtained when R79A is *not* pre-incubated with DNA (Table 4). Further, the rate constants obtained for protomer assembly (k_1) in both the nuclease assay (Table 2) and the ATPase assay (Table 4) are comparable, as anticipated if the assembly step is rate limiting for both reactions. These observations provide confidence that the proposed kinetic models adequately describe both the nuclease and ATPase reactions and we interpret the ensemble of kinetic data to indicate that change R79A results in a subtle defect in protomer assembly on DNA.

CONCLUSIONS

Sequence alignments suggest that residues K76, R79, G81, and S83 in lambda gpA are conserved and play critical roles in many viral terminases (46). Supporting this prediction, and consistent with the proposed roles of these residues, we find that residue changes at these positions caused strong impairments in virus yield, DNA translocation, and ATPase activities.

Eight of the twelve mutants surveyed by the single molecule assays spanning the motif were identified as exhibiting diverse partly-active translocation phenotypes that shed light on the roles of conserved and non-conserved residues and illustrate connections between tight ATP binding/hydrolysis states and DNA binding/translocation states. A simple model for the hydrolysis-translocation cycle that can account for all of our findings, summarizing the considerations discussed in the results section, is shown in Fig. 9A. The various roles ascribed to P-loop residues are summarized in Fig. 9B. The functional motor is composed of four protomers bound to the DNA. We assume that as with phi29 each protomer translocates 2.5 bp of DNA with each ATP hydrolytic cycle, one-at-a-time, in a highly coordinated fashion; this assumption is supported by our finding that incorporation of a single inactive protomer abrogates translocation activity (54). Initially, TerL begins in the apo-ATP state with DNA weakly gripped (state 1). ATP then loosely docks into the binding pocket in a

[iii]This could represent an allosteric activation induced by oligomerization; however, because a number of ATPase proteins from the ASCE family (such as some helicases, proteases, phages within the terminase subfamily, etc.) form oligomeric complexes whose nucleotide-binding pockets are assembled at the interface of adjacent protomers, we posit that lambda terminase similarly assembles where catalytically competent ATP binding sites only become complete when TerL subunits bind to one another. Thus, the formation of a ring terminase complex would mean all the ATP binding sites at each TerL-TerL interface are catalytically competent.

diffusion controlled rate (state 2), which is followed by a conformational change in TerL that (i) positions the ATP for hydrolysis and (ii) causes tight DNA grip (state 3). After hydrolysis TerL temporarily retains both ADP and P_i (state 4) and we assume that the physical translocation of DNA is associated with phosphate release, based on studies of the phage phi29 motor (56) (state 5). ADP release returns the cycle to the starting point with TerL in the apo-ATP state and DNA weakly gripped.

Three off-pathway states are considered to explain motor pausing and slipping. In pause state P1, occurring for WT and mutants V80A, G81A, and S83A, TerL grips DNA tightly but does not have ATP bound (apo-ATP state). Decreasing [ATP] increases the residence time of the WT motor in state 1, which decreases motor velocity, increases slipping because state 1 has weak DNA grip, and increases pausing due to an increased chance to transition to state P1. At saturating [ATP], structural perturbations caused by residue changes V80A, G81A, and S83A increase residence time in state 1 and/or 2, which decreases motor velocity, increases slipping frequency because TerL has weak DNA grip in these states, and increases pausing frequency due to an increased chance to transition to state P1[iv]. Residues V80, G81, and S83 are implicated in ATP docking/binding.

In pause state P2, occurring frequently for mutants A78V and R79K, TerL binds ATP tightly and undergoes a conformational change, but ATP is bound in a misaligned orientation and hydrolysis is very slow. Translocation pauses until the ATP aligns or dissociates and rebinds in a proper orientation. The frequent slipping exhibited by mutants A78V and R79K is attributed to an off-pathway state DC (“Defective Coupling”) in which ATP binds tightly but the coupling to DNA gripping fails. Residues A78 and R79 are implicated as playing important roles in ATP alignment and mechanochemical coupling, consistent with recent structure-based models (17, 18). We note that some slips occur immediately after pauses. The occurrence of such events was similar for WT and most mutants, but ~2-fold more frequent for A78V. This suggests it is also possible to transition directly from pause state P2 to state DC.

Residue changes Y82A and S83T decrease the residence time in states 1 and/or 2, which decreases slipping and pausing relative to WT; thus, Y82 is also implicated in ATP docking/binding. The reductions in motor velocity caused by residue changes A78V, R79K, Y82A, S83T, and K84A are attributed to slowed hydrolysis and/or ADP release. Notably, residues A78V and R79 are implicated in multiple roles: ATP alignment, ATP hydrolysis, and mechanochemical coupling. In addition, our biochemical studies of the R79A mutant enzyme reveal an identical kinetic lag in the time course for both *cos* cleavage and ATPase reactions, which we attribute to a common assembly defect. This implicates the Walker-A motif, and specifically R79 in ring tetramer assembly on DNA to engender a functional maturation complex, and perhaps for tight duplex gripping during the translocation cycle. This is consistent with recent structural models for the terminases of phages P74-26 and

[iv]It is possible that mutants with increased slipping could alternatively have a weaker DNA grip in the ATP tightly bound state, but since WA residues aren‘t thought to be directly contacting and gripping the DNA, we favor the interpretation that the mutations are affecting the residence time in the weak/strong gripping states. Slipping is expected to increase with increasing applied force, as we demonstrated with phage phi29 WT motor (9). We have compared mutants vs. WT at a single force, so any difference must be attributed to the residue changes.

phi29 which propose that the P-loop lies at the interface between motor subunits in the ring (18, 27), as has been found to occur in many other types of ring ATPases (29).

Our previous measurements showed that the DNA packaging motors of three different phages exhibit substantially different maximum motor velocities: ~150 bp/s for phi29 (which packages a ~19 kbp genome), ~400 bp/s for lambda (~49 kbp genome), and ~700 bp/s for T4 (~171 kbp genome) measured in saturating ATP at room temperature at the beginning of packaging. Our present finding that changes in non-conserved Walker A-region residues V80, A78, and Y82, and K84 cause relatively modest effects in motor velocity (35–68% of WT) suggest that changes in such residues during evolution could serve to tune motor velocity to the needs of different viruses. We also find that, higher initiation efficiency generally correlates with higher motor velocity. However, our finding with mutant Y82A indicate that high motor processivity can compensate for low motor velocity to enable high initiation efficiency.

Homology modeling predicts a lambda TerL Walker A motif with critical residues appropriately oriented for ATP phosphate binding and hydrolysis (Fig. 10). In general, residues 76–83 exhibit a loop structure common of P-loop motifs where the orientation of the residues produce an empty pocket that is available for the ATP phosphates to reside. Also, the serine from the Walker A sequence and the aspartate and glutamate residues from the Walker B motif appropriately point toward the Mg^{2+} for tight ATP binding and hydrolysis. Residue R79, on the other hand, points away from the ATP phosphates, but can be envisioned to rotate toward these phosphates, which could cause a conformational change to TerL similar to that proposed in the structural model of the phage P74-26 terminase.

More comprehensive future studies of the partly-active mutants we identified, as well as studies of the many other mutants we identified in our genetic assays that exhibit impairments in virus yield will certainly shed additional light on the mechanisms of the viral packaging motor. Such studies would be useful in affirming the proposed roles of residues and/or revealing additional roles of residues within the phosphate binding motif and to directly test specific aspects of our proposed kinetic model. In addition, as we demonstrated here, more detailed biochemical analyses can also be performed on any given mutant to provide greater insight on the roles of individual residues in the Walker A motif, as well as other functionally important regions of the motor protein.

MATERIALS AND METHODS

Supplementary methods includes descriptions of (1) microbiological methods (media, bacterial strains, mutagenesis, complementation assays, and *in vitro* screening); (2) biophysical methods (measurements of single DNA molecule packaging with optical tweezers); and (3) biochemical methods (DNA cleavage assays, circular dichroism, analytical ultracentrifugation, bulk in vitro packaging, and ATPase assays).

Supplementary Material

Refer to Web version on PubMed Central for supplementary material.

Acknowledgments

We thank Dr. David Baker (Univ. of Washington) for access to the CD spectrometer. This work was supported by NIH award R01-GM088186.

References

1. Earnshaw WC, Casjens SR. DNA packaging by the double-stranded DNA bacteriophages. Cell. 1980; 21(2):319–331. [PubMed: 6447542]
2. Smith DE, et al. The bacteriophage phi29 portal motor can package DNA against a large internal force. Nature. 2001; 413(6857):748–752. [PubMed: 11607035]
3. Fuller DN, et al. Measurements of single DNA molecule packaging dynamics in bacteriophage lambda reveal high forces, high motor processivity, and capsid transformations. J Mol Biol. 2007; 373(5):1113–1122. [PubMed: 17919653]
4. Fuller DN, Raymer DM, Kottadiel VI, Rao VB, Smith DE. Single phage T4 DNA packaging motors exhibit large force generation, high velocity, and dynamic variability. Proc Nat Acad Sci USA. 2007; 104(43):16868–16873. [PubMed: 17942694]
5. Fuller DN, et al. Ionic effects on viral DNA packaging and portal motor function in bacteriophage phi 29. Proc Nat Acad Sci USA. 2007; 104(27):11245–11250. [PubMed: 17556543]
6. Rickgauer JP, et al. Portal motor velocity and internal force resisting viral DNA packaging in bacteriophage phi29. Biophys J. 2008; 94(1):159–167. [PubMed: 17827233]
7. Smith DE. Single-molecule studies of viral DNA packaging. Current Opinion in Virology. 2011; 1:134. [PubMed: 22440623]
8. Chemla, YR.; Smith, DE. Single-molecule studies of viral DNA packaging. In: Rao, V.; Rossmann, MG., editors. Viral Molecular Machines. Springer; New York, NY: 2012. p. 549-584.
9. Berndsen ZT, Keller N, Smith DE. Continuous Allosteric Regulation of a Viral Packaging Motor by a Sensor that Detects the Density and Conformation of Packaged DNA. Biophys J. 2015; 108(2): 315–324. [PubMed: 25606680]
10. Berndsen ZT, Keller N, Grimes S, Jardine PJ, Smith DE. Nonequilibrium dynamics and ultraslow relaxation of confined DNA during viral packaging. Proc Nat Acad Sci USA. 2014; 111:8345–8350. [PubMed: 24912187]
11. Keller N, Grimes S, Jardine PJ, Smith DE. Repulsive DNA-DNA interactions accelerate viral DNA packaging in phage phi29. Phys Rev Lett. 2014; 112(24):248101. [PubMed: 24996111]
12. Migliori AD, et al. Evidence for an electrostatic mechanism of force generation by the bacteriophage T4 DNA packaging motor. Nature Communications. 2014; 5:4173.
13. Moffitt JR, et al. Intersubunit coordination in a homomeric ring ATPase. Nature. 2009; 457(7228): 446–450. [PubMed: 19129763]
14. Sun S, et al. The Structure of the Phage T4 DNA Packaging Motor Suggests a Mechanism Dependent on Electrostatic Forces. Cell. 2008; 135(7):1251–1262. [PubMed: 19109896]
15. Yu J, Moffitt J, Hetherington CL, Bustamante C, Oster G. Mechanochemistry of a viral DNA packaging motor. J Mol Biol. 2010; 400(2):186–203. [PubMed: 20452360]
16. Black LW. Old, new, and widely true: The bacteriophage T4 DNA packaging mechanism. Virology. 2015; 479:650–656. [PubMed: 25728298]
17. Zhao H, Christensen TE, Kamau YN, Tang L. Structures of the phage Sf6 large terminase provide new insights into DNA translocation and cleavage. Proc Nat Acad Sci USA. 2013; 110(20):8075–8080. [PubMed: 23630261]
18. Hilbert BJ, et al. Structure and mechanism of the ATPase that powers viral genome packaging. Proc Natl Acad Sci U S A. 2015; 112(29):E3792–3799. [PubMed: 26150523]
19. Harvey SC. The scrunchworm hypothesis: Transitions between A-DNA and B-DNA provide the driving force for genome packaging in double-stranded DNA bacteriophages. J Struc Biol. 2015; 189(1):1–8.
20. Casjens SR. The DNA-packaging nanomotor of tailed bacteriophages. Nature Reviews Microbiology. 2011; 9(9):647–657. [PubMed: 21836625]

21. Feiss, M.; Catalano, C. Bacteriophage lambda terminase and the mechanism of viral DNA packaging. In: Catalano, C., editor. Viral genome packaging machines: Genetics, structure and mechanism. Landes Bioscience; 2005.
22. Feiss, M.; Rao, VB. The bacteriophage DNA packaging machine. In: Rao, V.; Rossmann, MG., editors. Viral Molecular Machines. Springer; New York, NY: 2012. p. 489-509.
23. Black LW, Rao VB. Structure, assembly, and DNA packaging of the bacteriophage T4 head. Adv Virus Res. 2012; 82:119. [PubMed: 22420853]
24. Maluf NK, Yang Q, Catalano CE. Self-association properties of the bacteriophage lambda terminase holoenzyme: Implications for the DNA packaging motor. J Mol Biol. 2005; 347(3):523–542. [PubMed: 15755448]
25. Yang TC, Catalano CE, Maluf NK. Analytical Ultracentrifugation as a Tool to Study Nonspecific Protein-DNA Interactions. Methods Enzymol. 2015; 562:305–330. [PubMed: 26412658]
26. Maluf NK, Gaussier H, Bogner E, Feiss M, Catalano CE. Assembly of bacteriophage lambda terminase into a viral DNA maturation and packaging machine. Biochemistry. 2006; 45(51): 15259–15268. [PubMed: 17176048]
27. Mao H, et al. Structural and Molecular Basis for Coordination in a Viral DNA Packaging Motor. Cell Rep. 2016; 14(8):2017–2029. [PubMed: 26904950]
28. Burroughs AM, Iyer LM, Aravind L. Comparative genomics and evolutionary trajectories of viral ATP dependent DNA-packaging systems. Genome dynamics. 2007; 3:48–65. [PubMed: 18753784]
29. Lyubimov AY, Strycharska M, Berger JM. The nuts and bolts of ring-translocase structure and mechanism. Curr Opin Struct Biol. 2011; 21(2):240–248. [PubMed: 21282052]
30. Allemand J-F, Maier B, Smith DE. Molecular motors for DNA translocation in prokaryotes. Current opinion in biotechnology. 2012; 23(4):503–509. [PubMed: 22226958]
31. Saraste M, Sibbald PR, Wittinghofer A. The P-loop--a common motif in ATP- and GTP-binding proteins. Trends Biochem Sci. 1990; 15(11):430–434. [PubMed: 2126155]
32. Walker JE, Saraste M, Runswick MJ, Gay NJ. Distantly related sequences in the alpha- and beta-subunits of ATP synthase, myosin, kinases and other ATP-requiring enzymes and a common nucleotide binding fold. EMBO J. 1982; 1(8):945–951. [PubMed: 6329717]
33. Kjeldgaard M, Nyborg J. Refined structure of elongation factor EF-Tu from Escherichia coli. J Mol Biol. 1992; 223(3):721–742. [PubMed: 1542116]
34. Pai EF, et al. Structure of the guanine-nucleotide-binding domain of the Ha-ras oncogene product p21 in the triphosphate conformation. Nature. 1989; 341(6239):209–214. [PubMed: 2476675]
35. Müller CW, Schulz GE. Structure of the complex between adenylate kinase from Escherichia coli and the inhibitor Ap5A refined at 1.9 A resolution. A model for a catalytic transition state. J Mol Biol. 1992; 224(1):159–177. [PubMed: 1548697]
36. Seefeldt LC. Docking of nitrogenase iron- and molybdenum-iron proteins for electron transfer and MgATP hydrolysis: the role of arginine 140 and lysine 143 of the Azotobacter vinelandii iron protein. Protein Sci. 1994; 3(11):2073–2081. [PubMed: 7703853]
37. Ryle MJ, Lanzilotta WN, Mortenson LE, Watt GD, Seefeldt LC. Evidence for a central role of lysine 15 of Azotobacter vinelandii nitrogenase iron protein in nucleotide binding and protein conformational changes. J Biol Chem. 1995; 270(22):13112–13117. [PubMed: 7768906]
38. Cremo CR, Grammer JC, Yount RG. Direct chemical evidence that serine 180 in the glycine-rich loop of myosin binds to ATP. J Biol Chem. 1989; 264(12):6608–6611. [PubMed: 2523383]
39. Rao VB, Feiss M. The Bacteriophage DNA Packaging Motor. Ann Rev Genetics. 2008; 42:647–681. [PubMed: 18687036]
40. Mitchell MS, Matsuzaki S, Imai S, Rao VB. Sequence analysis of bacteriophage T4 DNA packaging/terminase genes 16 and 17 reveals a common ATPase center in the large subunit of viral terminases. Nucleic Acids Res. 2002; 30(18):4009–4021. [PubMed: 12235385]
41. Kondabagil K, Draper B, Rao VB. Adenine recognition is a key checkpoint in the energy release mechanism of phage T4 DNA packaging motor. J Mol Biol. 2012; 415(2):329–342. [PubMed: 22100308]

42. Hang JQ, Tack BF, Feiss M. ATPase center of bacteriophage lambda terminase involved in post-cleavage stages of DNA packaging: Identification of ATP-interactive amino acids. J Mol Biol. 2000; 302(4):777–795. [PubMed: 10993723]
43. Dhar A, Feiss M. Bacteriophage lambda terminase: Alterations of the high-affinity ATPase affect viral DNA packaging. J Mol Biol. 2005; 347(1):71–80. [PubMed: 15733918]
44. Tsay JM, Sippy J, Feiss M, Smith DE. The Q motif of a viral packaging motor governs its force generation and communicates ATP recognition to DNA interaction. Proc Nat Acad Sci USA. 2009; 106(34):14355–14360. [PubMed: 19706522]
45. Duffy C, Feiss M. The large subunit of bacteriophage lambda's terminase plays a role in DNA translocation and packaging termination. J Mol Biol. 2002; 316(3):547–561. [PubMed: 11866517]
46. Mitchell MS, Rao VB. Novel and deviant Walker A ATP-binding motifs in bacteriophage large terminase-DNA packaging proteins. Virology. 2004; 321(2):217–221. [PubMed: 15051382]
47. Draper B, Rao VB. An ATP hydrolysis sensor in the DNA packaging motor from bacteriophage T4 suggests an inchworm-type translocation mechanism. J Mol Biol. 2007; 369(1):79–94. [PubMed: 17428497]
48. Mitchell MS, Rao VB. Functional analysis of the bacteriophage T4 DNA-packaging ATPase motor. J Biol Chem. 2006; 281(1):518–527. [PubMed: 16258174]
49. Rao VB, Mitchell MS. The N-terminal ATPase site in the large terminase protein gp17 is critically required for DNA packaging in bacteriophage T4. Journal of Molecular Biology. 2001; 314(3): 401–411. [PubMed: 11846554]
50. Tsay JM, et al. Mutations altering a structurally conserved loop-helix-loop region of a viral packaging motor change DNA translocation velocity and processivity. J Biol Chem. 2010; 285(31):24282–24289. [PubMed: 20525695]
51. delToro D, Smith DE. Accurate measurement of force and displacement with optical tweezers using DNA molecules as metrology standards. Appl Phys Lett. 2014; 104(14):143701. [PubMed: 25316922]
52. Fuller DN, et al. A general method for manipulating DNA sequences from any organism with optical tweezers. Nucleic Acids Res. 2006; 34(2):e15. [PubMed: 16452295]
53. Rickgauer JP, Fuller DN, Smith DE. DNA as a metrology standard for length and force measurements with optical tweezers. Biophys J. 2006; 91(11):4253–4257. [PubMed: 16963512]
54. Andrews BT, Catalano CE. Strong subunit coordination drives a powerful viral DNA packaging motor. Proc Nat Acad Sci USA. 2013; 110(15):5909–5914. [PubMed: 23530228]
55. Chistol G, et al. High degree of coordination and division of labor among subunits in a homomeric ring ATPase. Cell. 2012; 151(5):1017–1028. [PubMed: 23178121]
56. Chemla YR, et al. Mechanism of force generation of a viral DNA packaging motor. Cell. 2005; 122(5):683–692. [PubMed: 16143101]
57. Tomka MA, Catalano CE. Kinetic characterization of the ATPase activity of the DNA packaging enzyme from bacteriophage lambda. Biochemistry. 1993; 32(45):11992–11997. [PubMed: 8218275]
58. Hwang Y, Catalano CE, Feiss M. Kinetic and mutational dissection of the two ATPase activities of terminase, the DNA packaging enzyme of bacteriophage Chi. Biochemistry. 1996; 35(8):2796–2803. [PubMed: 8611586]
59. McClure WR. Mechanism and control of transcription initiation in prokaryotes. Annu Rev Biochem. 1985; 54:171–204. [PubMed: 3896120]
60. Simpson AA, et al. Structure of the bacteriophage phi29 DNA packaging motor. Nature. 2000; 408(6813):745–750. [PubMed: 11130079]
61. Lhuillier S, et al. Structure of bacteriophage SPP1 head-to-tail connection reveals mechanism for viral DNA gating. Proceedings of the National Academy of Sciences of the United States of America. 2009; 106(21):8507–8512. [PubMed: 19433794]
62. Vafabakhsh R, et al. Single-molecule packaging initiation in real time by a viral DNA packaging machine from bacteriophage T4. Proceedings of the National Academy of Sciences of the United States of America. 2014; 111(42):15096–15101. [PubMed: 25288726]

63. Andrews BT, Catalano CE. The enzymology of a viral genome packaging motor is influenced by the assembly state of the motor subunits. Biochemistry. 2012; 51(46):9342–9353. [PubMed: 23134123]

64. Yang TC, Ortiz D, Nosaka L, Lander GC, Catalano CE. Thermodynamic Interrogation of the Assembly of a Viral Genome Packaging Motor Complex. Biophys J. 2015; 109(8):1663–1675. [PubMed: 26488657]

65. von Hippel PH, Berg OG. Facilitated target location in biological systems. J Biol Chem. 1989; 264(2):675–678. [PubMed: 2642903]

66. Yang Q, Hanagan A, Catalano CE. Assembly of a nucleoprotein complex required for DNA packaging by bacteriophage lambda. Biochemistry. 1997; 36(10):2744–2752. [PubMed: 9062101]

67. Yang Q, Catalano CE. Biochemical characterization of bacteriophage lambda genome packaging in vitro. Virology. 2003; 305(2):276–287. [PubMed: 12573573]

68. Yang Q, Catalano CE, Maluf NK. Kinetic Analysis of the Genome Packaging Reaction in Bacteriophage lambda. Biochemistry. 2009; 48(45):10705–10715. [PubMed: 19788336]

69. Zhang Y. I-TASSER server for protein 3D structure prediction. BMC Bioinformatics. 2008; 9:40. [PubMed: 18215316]

Highlights

- Detailed structure-function mechanisms of viral packaging motors remain unclear
- Study of an extensive collection of mutants shows P-loop residues play critical roles
- Residues are implicated in ATP binding, mechanochemical coupling, and motor assembly
- Biochemical and biophysical measurements provide support for recent structural models
- The P-loop plays key roles in coordinating ATP hydrolysis with DNA translocation

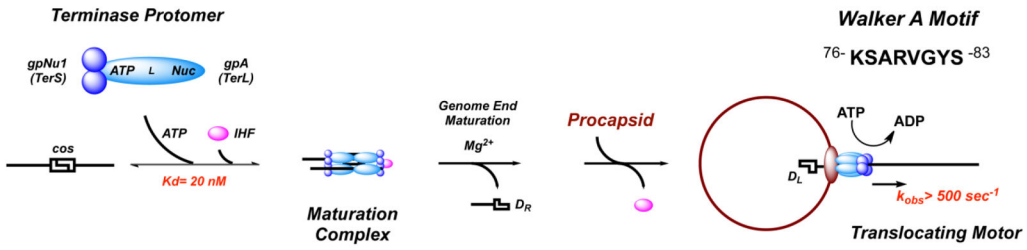

Figure 1. The lambda genome packaging pathway

The terminase protomer is composed of two gpNu1 subunits tightly associated with one gpA subunit (gpA_1•$gpNu1_2$). The N-terminal domain in gpA contains the packaging ATPase catalytic site (ATP) while the C-terminal domain contains the *cos*-cleavage nuclease activity responsible for genome maturation (Nuc); the two domains are connected by a linker domain (L). The protomer is devoid of catalytic activity. Four protomers assemble into a ring-like structure at the *cos* site of a lambda genome concatemer to afford the activated maturation complex [(gpA_1•$gpNu1_2$)$_4$]; this assembly step requires ATP and/or IHF. Duplex nicking by gpA and ejection of the upstream D_R end yields the post-cleavage complex, which binds to the portal of an empty procapsid to yield the packaging motor complex. This activates the packaging ATPase site, which powers translocation of DNA into the procapsid shell; the TerS dimer seen in the motor-procapsid complex on the right is depicted as a single sphere for simplicity. We note that the conformation of the tetramer stoichiometry and the conformation of the protomer subunits bound to the procapsid remains speculative at this time.

Φ yield (pfu/cell) (Relative to WT)	Color Key
$1 \sim 10^{-1}$	
$10^{-1} \sim 10^{-2}$	
$10^{-2} \sim 10^{-3}$	
$10^{-3} \sim 10^{-5}$	
$10^{-5} \sim 10^{-7}$	
$< 10^{-7}$	

Figure 2A

Figure 2a

K_{76}	S_{77}	A_{78}	R_{79}	V_{80}	G_{81}	Y_{82}	S_{83}	K_{84}
A	G	V	A	L	A	H	T	R
H	N	P	E	A	L	F	K	C
I	V	F	G	K	I	G	A	A
P	P	G	H	N	K	A	C	S
R	T	H	K	Q	P	C	E	G
S	F	I	L	S	R	E	I	L
T	H	K	N	G	T	P	L	N
V	L	L	P	P	W	R	P	V
W	R	Q	S	R		T	Q	D
		R	Y			V	V	I
		S					W	T

Figure 2B

Figure 2b

Figure 2. Impairments in viral assembly caused by residue changes in the Walker A motif in the DNA translocation ATPase of the phage lambda large terminase subunit

(A) Range of detected degrees of impairment expressed in terms of phage yield in plaque forming units per cell relative to WT (where the WT activity is defined to be 1). Note that

the gray color is used to designate cases where no phage yield was detected (*i.e.*, below the level of sensitivity of the assay). (B) Chart listing measured activity levels in response to each single residue change tested. The 1st row lists the residues that were changed and the cells in other rows list the substituted residue and the color of each cell indicates the activity level corresponding to that residue change. The underlined residues are those observed to be highly conserved in a “Deviant I” Walker A-like motif subfamily (46). Note that K84 lies just outside the motif; to indicate this we have shaded its box white.

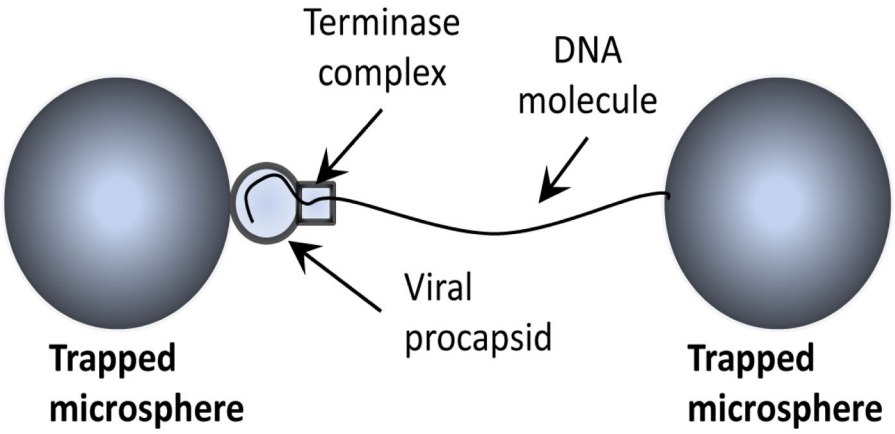

Figure 3A

Figure 3a

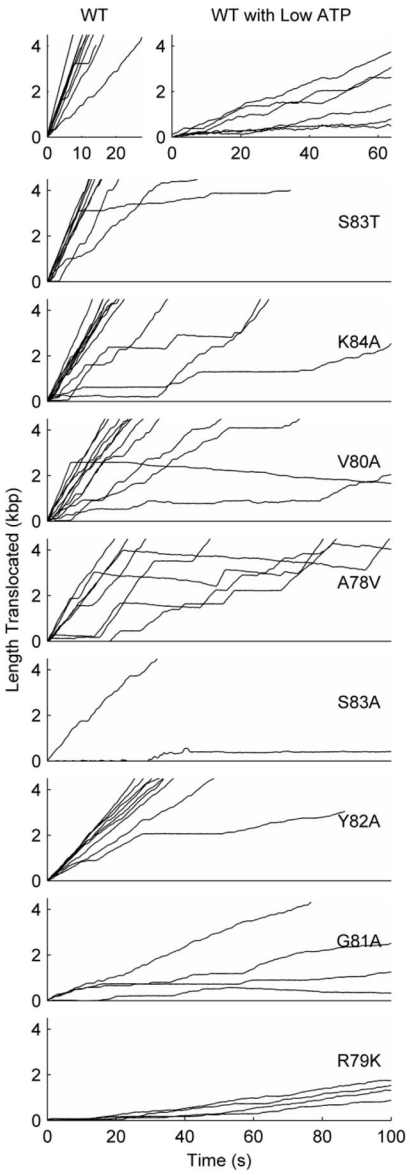

Figure 3B

Figure 3b

Figure 3. (A) Optical Tweezers Assay

Within an ATP-buffer filled flow chamber, a single viral prohead-motor-DNA complex is tethered between two trapped microspheres. During packaging of the DNA into the prohead, a force feedback control maintains a 5pN load on the tethered complex while the separation between the beads is recorded. **(B) Translocation dynamics.** Measurements of length of DNA packaged vs. time for WT and mutant terminases under a 5 pN applied load at low procapsid filling (<10% of genome length packaged). Each plot shows ~10 typical examples

of packaging events (or fewer for mutants that initiated very inefficiently and for which fewer than 10 events were recorded). The upper left plot shows WT with saturating ATP (0.5 mM) and the upper right one shows WT with low ATP (2.5 μM). All of the mutants were measured with 0.5 mM ATP. All plots have the same x- and y-axis scale sizes.

Terminase	Motor Velocity (bp/s)	Packaging Rate (bp/s)	Initiation Efficiency (% of WT)	Pauses per kbp DNA packaged	Pause Duration (s)	Slips per kbp DNA packaged	# of Events	phage yield
WT	400 ± 20	350 ± 20	100 ± 10	1.2 ± 0.4	2 ± 0.1	0.5 ± 0.1	53	1
S83T	340 ± 10	300 ± 20	60 ± 20	0.5 ± 0.1	2 ± 0.4	0.09 ± 0.01	44	4×10^{-5}
K84A	270 ± 20	220 ± 20	60 ± 10	1.3 ± 0.3	2.2 ± 0.3	0.3 ± 0.1	34	5.7×10^{-3}
V80A	230 ± 10	160 ± 20	80 ± 10	5 ± 1	4.4 ± 0.3	3 ± 1	51	6.7×10^{-3}
A78V	173 ± 8	36 ± 7	55 ± 5	14 ± 2	4.5 ± 0.2	11 ± 1	61	1×10^{-3}
S83A	170 ± 10	80 ± 70	5 ± 3	6 ± 4	2 ± 0.4	5 ± 5	2	$< 10^{-7}$
Y82A	138 ± 6	132 ± 7	90 ± 10	1 ± 0.3	1.4 ± 0.5	0.11 ± 0.5	23	6.7×10^{-3}
WT 5μM ATP	130 ± 20	50 ± 20	27 ± 8	8 ± 2	1.58 ± 0.09	5 ± 1	9	
WT 2.5μM ATP	79 ± 6	24 ± 7	35 ± 3	13 ± 2	1.8 ± 0.1	7 ± 1	13	
G81A	62 ± 8	23 ± 12	8 ± 5	23 ± 9	3.4 ± 0.5	9 ± 8	4	1.4×10^{-5}
R79K	42 ± 3	13 ± 2	5 ± 3	24 ± 2	3.4 ± 0.3	1.3 ± 0.5	5	$< 10^{-7}$
R79A	0	0	0	0	0	0	0	$< 10^{-7}$
S77V	0	0	0	0	0	0	0	1.3×10^{-3}
K76A	0	0	0	0	0	0	0	$< 10^{-7}$
K76R	0	0	0	0	0	0	0	$< 10^{-7}$

Figure 4. Metrics of DNA translocation activity

These metrics were determined by analysis of the optical tweezers measurements. For each mutant several hundred trials were performed to acquire these results. The other columns are reported as mean values, except for the last column which reports viral assembly activity (phage yield per cell) as a fraction of WT (the color codes in this column are the same as used in Fig. 2). All measurements were done with saturating ATP (0.5 mM) except for those labeled WT 5 μM ATP and WT 2.5 μM ATP, which report WT measurements with lowered [ATP]. Uncertainties are expressed as standard error in the mean.

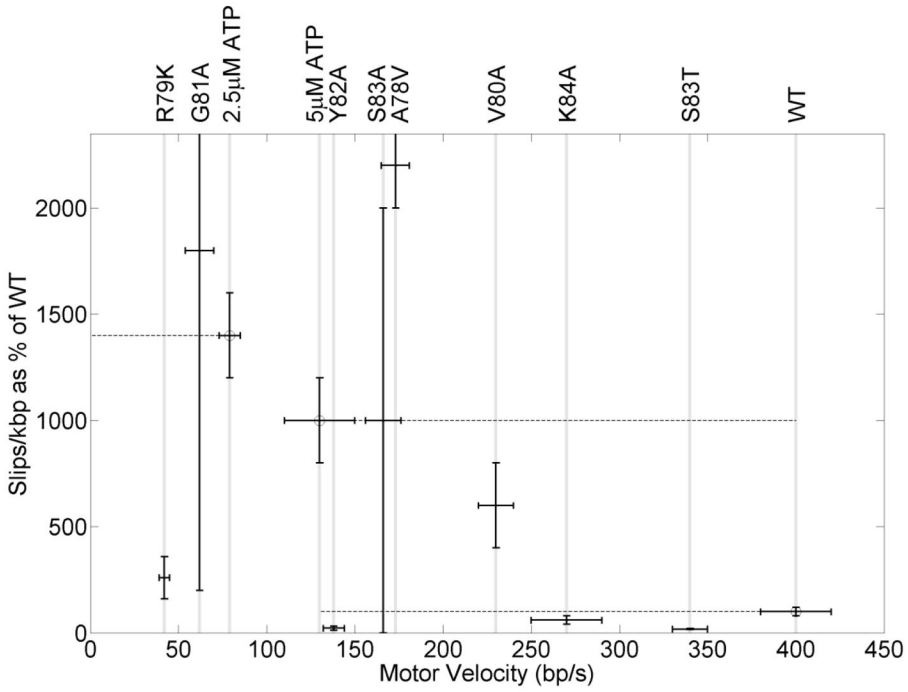

Figure 5A

Figure 5a

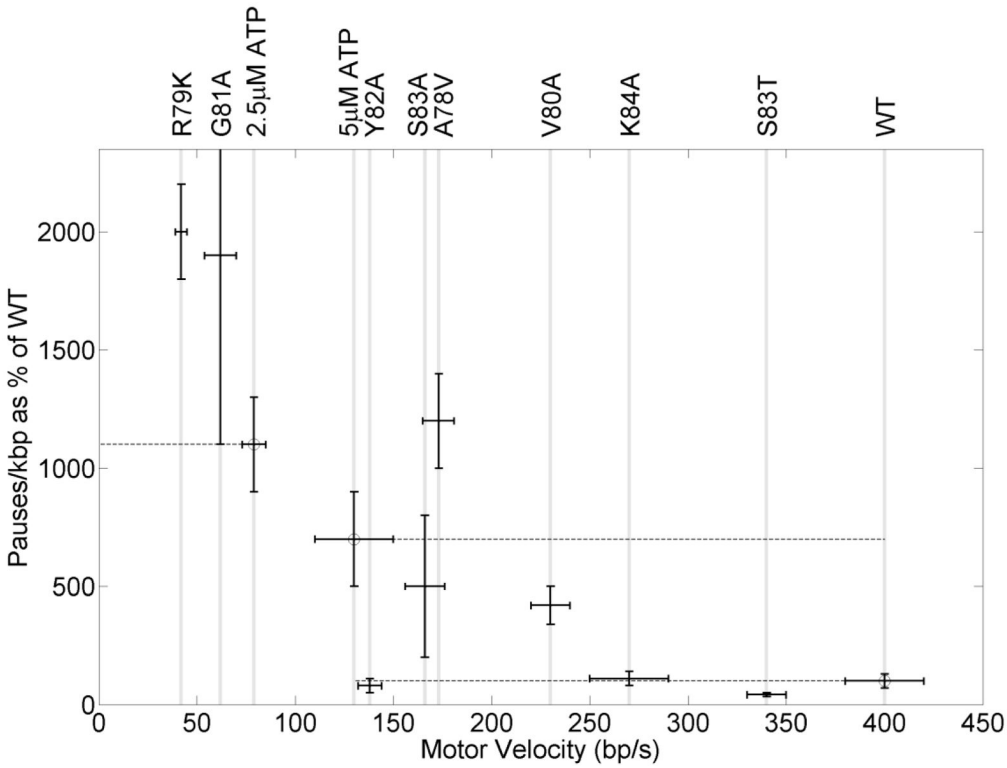

Figure 5B

Figure 5b

Figure 5. Frequencies of slipping (A) and pausing (B) vs motor velocity

The height of the points indicate the average amount of slipping or pausing per kbp of DNA packaged as a percentage of that exhibited by WT. Error bars indicate standard errors in the means. The light grey vertical lines have been included to help in labelling the points. All measurements were in saturating ATP (0.5 mM) except the two listed as 2.5 and 5 μM ATP, which indicate measurements with WT at these lower ATP concentrations. The three WT measurements are indicated by the open circles. Note that, for WT, slipping and pausing frequencies increase with decreasing motor velocity. Mutants that obey this same trend fall between the two dashed lines on the right (indicating slipping frequencies measured with WT in 5 μM and in 0.5 mM ATP), or above the dashed line on the left (indicating slipping frequency measured with WT in 2.5 μM ATP).

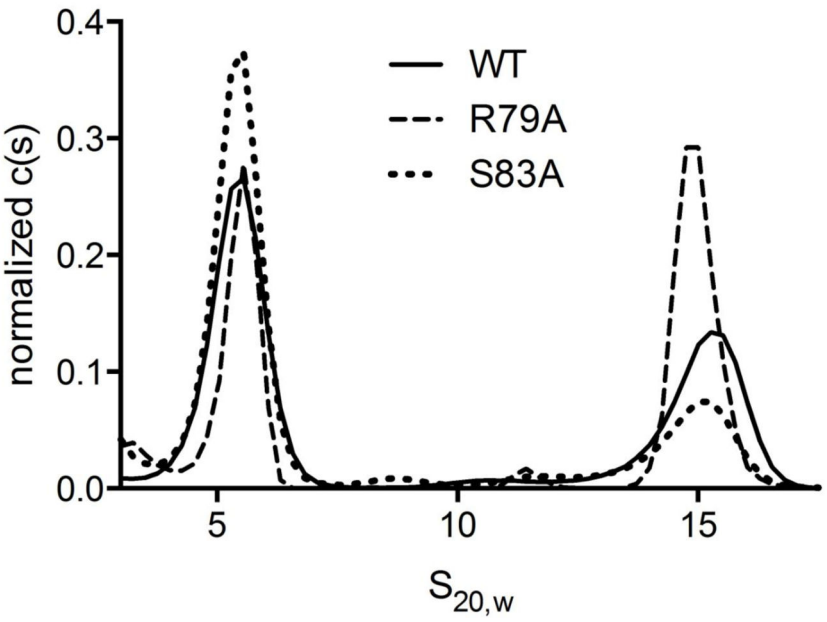

Figure 6. Assessment of motor-assembly

SV-AUC analysis indicates the Walker A mutants have no major assembly defects. The WT protomer (5S) is in slow equilibrium with a tetramer of protomers (~15S). The mutant enzyme similarly assemble, albeit at different ratios than WT (62% protomer for WT vs. 45% and 80% for R79A and S83A, respectively). This variability is consistent with prep-to-prep variability in WT enzyme.

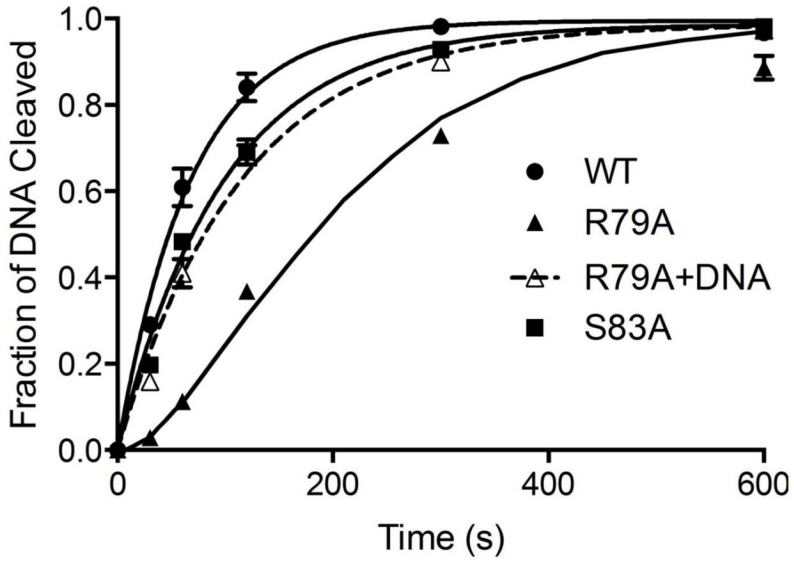

Figure 7. Kinetic analysis of *cos*-cleavage activity

The reaction time courses for WT (●) and S83A (■) are well described by a single-turnover, monophasic exponential model (solid lines), and indicate that S83A has a modest ~1.5-fold reduced k_{obs} relative to WT (k_{obs} =0.01 ± 0.001 s^{-1} and 0.015 ± 0.001 s^{-1}, respectively; Table 2). In contrast, R79A displays a significant lag phase (▲) and is better described by a 3-state mode that includes a slow step prior to catalysis (Equation 2, solid line). To investigate the nature of the lag, R79A was pre-incubated with *cos*DNA as described in *Methods* and the reaction was initiated with Mg^{2+} (△). This eliminates the lag phase and produces kinetic data well described as a monophasic exponential time course (dashed line). Under these conditions, the observed rate constant for R79A is similar to that of S83A (k_{obs} =0.009 ± 0.001 s^{-1}; Table 2). In all cases, the data points represent the average of experiments performed in triplicate, with error bars indicating standard errors in the mean.

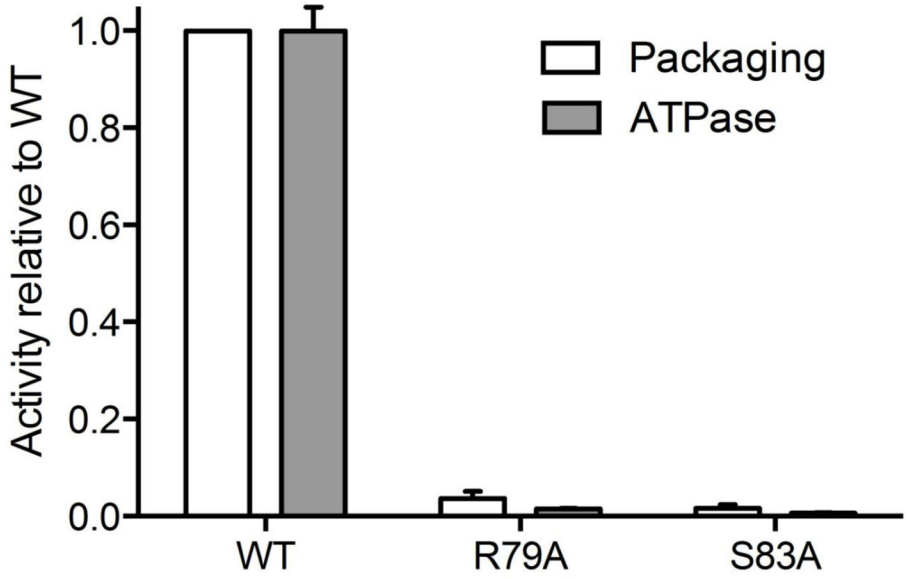

Figure 8A

Figure 8a

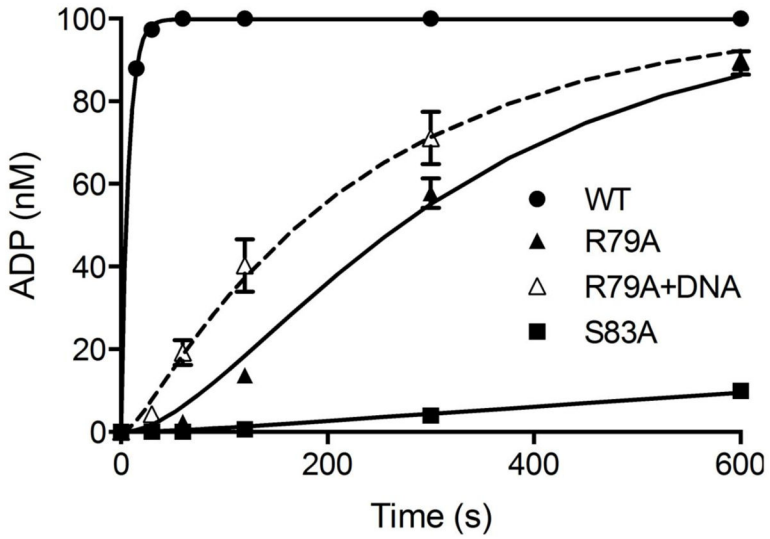

Figure 8B

Figure 8b

Figure 8. Kinetic analysis of packaging and ATPase activities

(A) Packaging and steady-state ATPase activities were sharply reduced for both mutants (n≥3). **(B)** Single turnover ATPase reactions were initiated by the addition of enzyme. R79A

displays a significant lag phase and the data are well described by a 3-state model that includes a slow step prior to hydrolysis. Pre-incubation of R79A with DNA (dashed line) greatly reduces the lag phase, suggesting DNA interactions are impaired. Pre-incubation of WT with DNA showed no effect on kinetics (data not shown).

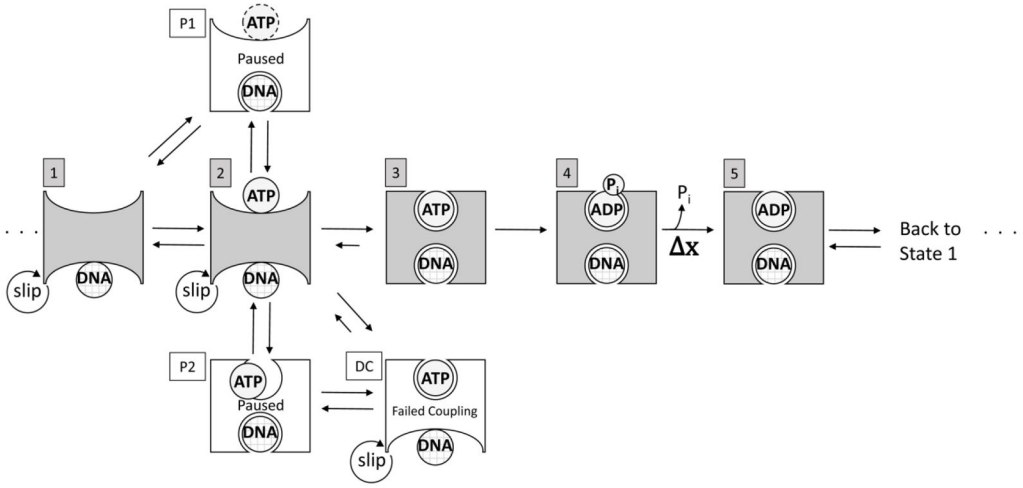

Figure 9A

Figure 9a

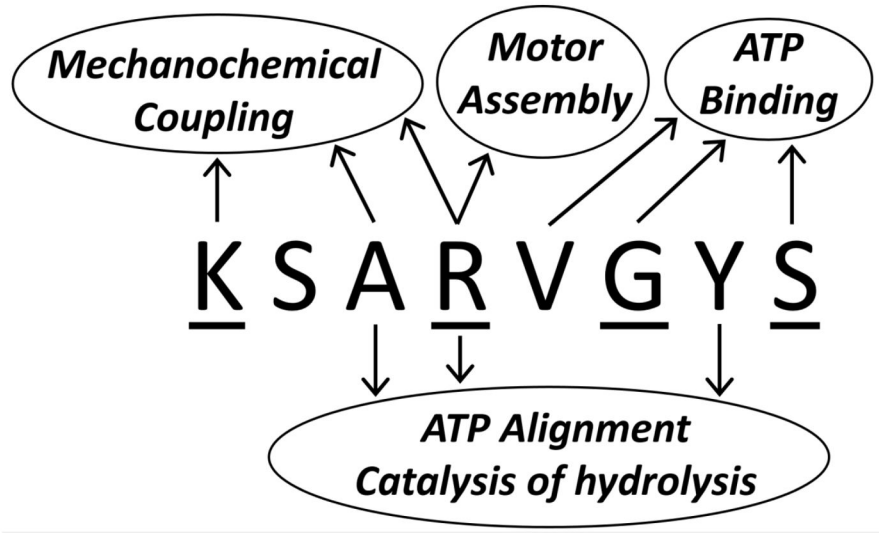

Figure 9B

Figure 9b

Figure 9. (A) Model for the mechanochemical kinetic cycle of a TerL subunit

As discussed in the text, the starting in the Apo (empty) state (state 1) the main on-pathway cycle proceeds with loose ATP docking (state 2), a conformational change of TerL induced by tight ATP binding (state 3), ATP hydrolysis (state 4), and phosphate release and translocation (state 5), and then ADP release (back to state 1). Three off-pathway states result in pausing and slipping. In pause state P1, occurring for WT and mutants V80A, G81A, and S83A, TerL grips DNA tightly but does not bind ATP tightly. In pause state P2,

occurring frequently for mutants A78V and R79K, TerL binds ATP tightly and undergoes a conformational change, but ATP is bound in a misaligned orientation and the motor pauses until the ATP aligns or dissociates and rebinds in a proper orientation. In state DC ("Defective Coupling"), occurring frequently for mutants A78V and R79K, ATP binds correctly but the coupling between ATP binding and DNA gripping fails, resulting in slipping. **(B) Diagram summarizing the various roles ascribed to the lambda terminase P-loop residues in the model**. We note that this diagram only lists roles supported by results presented in this article.

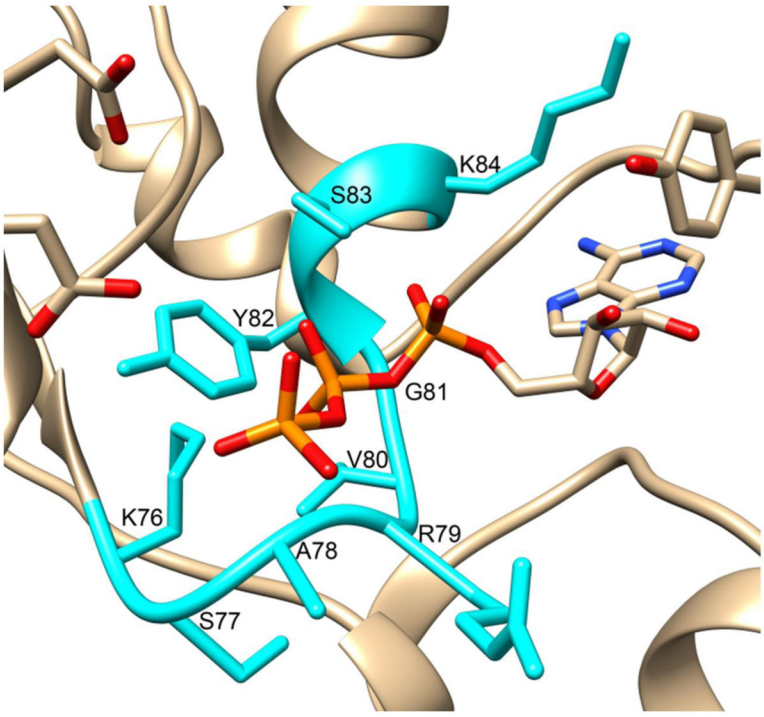

Figure 10. Structural homology model of lambda TerL
(created with I-TASSER) (69).

The N-terminal (packaging) ATPase site is shown here with an ATP molecule pre-docked by I-TASSER according to the docking position of structural homologs. The atypical Walker A P-loop and adjacent K84 are highlighted in cyan. The S83 hydroxyl group is adjacent to the β,γ phosphates, while the R79 side chain simultaneously interacts with the γ phosphate and the 'linker' domain, consistent with results presented here.

Table 1

Examples of known and putative Walker A motif sequences for the translocation ATPase in viral packaging motor proteins

Classically conserved Walker A residues are indicated in bold and additional residues proposed to be conserved in many viral terminases are underlined. The first four viruses are examples assigned to a “Deviant I” Walker-A-like motif subfamily (46). The others are representative examples in viruses that have been extensively studied.

Virus	Sequence	Ref.
Classical motif	(**G/A**)XXXX**GK**(**T/S**)	(30)
Lambda	76-KSARV**GYS**-83	(46)
21	76-KSARV**GYT**-83	(46)
P2	166-KSRQI**G**A**T**-173	(46)
Mu	64-KSRRT**G**L**T**-71	(46)
T4	160-LSRQL**GKT**-167	(46)
T5	62-VSRRV**GKS**-69	(39)
P74-26	37-LGRQS**GKS**-44	(18)
Sf6	22-**G**GRGS**GKS**-29	(17)
Phi29	24-**G**ARGI**GKS**-31	(39)
T3/T7	58-**A**FRGI**GKS**-65	(48)
P22	60-**A**GNQL**GKS**-67	(48)
HK97	54-IARKN**GKT**-61	(48)
SPP1	33-**G**GRGSA**KS**-40	(48)
HSV-1	258-VPRRH**GKT**-265	(48)

Table 2

Model parameters determined for kinetic *cos*-cleavage data

	***cos*-cleavage**		
	Monophasic Model (Equation 1)	**3-State Model (Equation 2)**	
	k_{obs} **(sec^{-1})**	k_1 **(M^{-1}sec^{-1})**	k_{obs} **(sec^{-1})**
WT	0.015 ± 0.001	---	---
S83A	0.010 ± 0.001	---	---
R79A	-	$(4.8 \pm 0.4) \times 10^4$	0.032 ± .008
R79A+DNA	0.009 ± 0.001	---	---

Table 3

Steady state ATPase activity

	Steady State Hydrolysis	Relative Activity
WT	k_{obs}= (0.457 ± 0.022) sec^{-1}	100%
S83A	k_{obs}= (3.2 ± 0.2) × 10^{-3} sec^{-1}	0.7%
R79A	k_{obs}= (7.0 ± 0.3) × 10^{-3} sec^{-1}	1.5%

Table 4

Single-turnover ATPase activity

Single-Turnover ATPase			
	Monophasic Model (Equation 1)	**3-State Model (Equation 3)**	
	k_{obs} (sec^{-1})	**k_1 ($M^{-1}sec^{-1}$)**	**k_2 (sec^{-1})**
WT	0.123 ± 0.001	$(1.0 \pm 0.65) \times 10^6$ M^{-1}	0.123 *(fixed)*
S83A	$(1.8 \pm 0.4) \times 10^{-4}$	---	---
R79A	---	$(1.32 \pm 0.9) \times 10^4$	$(5.3 \pm 2.9) \times 10^{-3}$
R79A+DNA	$(4.9 \pm 0.6) \times 10^{-3}$	---	---